



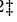


Title of submission to PLOS journals

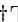
Name1 Surname^{1,2}, Name2 Surname², Name3 Surname^{2,3}, Name4 Surname²,
Name5 Surname², Name6 Surname², Name7 Surname^{1,2,3}^{*}, with the Lorem Ipsum Consortium[†]

1 Affiliation Dept/Program/Center, Institution Name, City, State, Country

2 Affiliation Dept/Program/Center, Institution Name, City, State, Country


3 Affiliation Dept/Program/Center, Institution Name, City, State, Country

 These authors contributed equally to this work.

 These authors also contributed equally to this work.

 Current Address: Dept/Program/Center, Institution Name, City, State, Country

 Deceased

 Membership list can be found in the Acknowledgments section.

* correspondingauthor@institute.edu

Abstract

The topology of cortical networks is subject to constant change and the mechanisms involved in these dynamics are strongly influenced by the timing and intensity of neural spiking within these networks. Consequently, the success of a realistic biologically based computational model of synaptic structure and self-organization largely depends on an accurate modeling of neural activity. Experiments have found evidence for a broad, log-normal distribution of firing rates among cortical neurons. It is suggested that this heterogeneity of cortical activity has a functional role in the context of stimulus encoding and the formation of stable subpopulations of synapses.

Building upon on a self-organizing spiking neural network (LIF-SORN), we replaced an intrinsic homeostatic control system used in earlier versions by a mechanism based on the diffusion of a neurotransmitter across the nervous tissue. Diffusive homeostasis was adopted from a paper by Sweeney et al. The main goal of this modification was to allow for the aforementioned broad and heavy tailed distribution of firing rates among the excitatory neural population, which could not be achieved by the formerly used single-cell homeostatic mechanism, binding firing rates of all neurons to a fixed target value. The resulting statistical features of spiking activity were positive regarding the desired firing rate statistics. Furthermore, we compared both homeostatic mechanisms with respect to features of synaptic network structures emerging throughout the simulation. Apart from the preservation of earlier reported non-random topological features, we found that diffusive homeostasis allowed for the emergence of highly influential neurons with strong outgoing synaptic efficacies. We could relate this feature of synaptic topology to the imposed spatial structure of the neural population by means of an analytic approach to the diffusive homeostatic steady state.

Author summary

We improved a model of cortical self-organization and activity by implementing a diffusive mechanism of feedback control. Previously reported non-random topological

features of the network were preserved while allowing for a broader distribution of firing rates. Our modifications also led to the accumulation of strong synapses to a small subgroup of highly active presynaptic neurons. By further analyzing the feedback control, we found that the statistics of firing rates within the network is strongly affected by the structure of the neurons' positions. This raises the question if the spatial structure of a cortical network can actually shape activity not only by means of distance-dependent synaptic connection probabilities, but also through diffusive interaction.

Introduction

Many theoretical studies in recent years have addressed the question how cortical network activity and synaptic structure forms and organizes itself, based on a limited set of experimentally observed basic mechanisms and compartments [1–4]. Typical compartments of these models include some type of hebbian-type rule of synaptic plasticity, especially spike-timing-dependent plasticity in the case of spiking networks [5], and some type of control that limits synaptic efficacies, usually by postsynaptic scaling [6]. It is believed that the so-called *balanced state* of such a network, which is characterized by an irregular, weakly correlated spiking pattern, reproduces the characteristics of experimentally observed spiking activity in the cortex [7]. This state of activity requires a stable balance between excitation and inhibition. Since network topology is subject to constant change, some form of stabilizing, homeostatic feedback control has to be implemented in order to maintain this equilibrium. While recent theoretical studies have argued that stabilization of recurrent networks is achieved by the presence of inhibitory plasticity [8], common forms of homeostasis are believed to take place either through the modulation of excitatory synapses [9], or by modifications of intrinsic neuronal excitability [10]. Previous research on a binary self-organizing recurrent neural network (SORN) by Lazar et al. [1] and a more biologically realistic spiking version of this network (LIF-SORN) by Miner and Triesch [11] used an intrinsic homeostatic control mechanism to regulate excitatory activity on a single-cell level. Despite this very simple form of homeostatic control, the network has proven to be capable of showing a number of experimentally confirmed non-random features. Zheng et al. have shown that distribution and dynamics of synaptic efficacies measured in rat hippocampus can be reproduced by a binary SORN using a discretized version of spike-timing-dependent plasticity and presynaptic normalization [12]. With the LIF-SORN, Miner et al. reproduced the results of the binary SORN regarding self-organizing synaptic dynamics. Furthermore, they were able to explain the experimentally observed overrepresentation of bidirectional connections [13,14] by means of a distance-dependent implementation of synaptic growth. The SORN's ability of self-organization has not only been investigated in terms of network structure itself. It also successfully performed in unsupervised sequence-learning tasks, suggesting that it can acquire and maintain associative memory [15].

As mentioned above, previous versions of our recurrent network model regulated activity by fixing excitatory firing rates to a predefined target value. However, strong evidence exists for a log-normal like distribution of cortical firing rates [16,17]. Experimental and theoretical studies have suggested that the presence of both slow- and fast-firing cells is not to be regarded as an ignorable, mere side effect of brain dynamics. It rather seems to be that skewed and heavy-tailed firing rate statistics are necessary with respect to the preservation of stable synaptic structures being related to long-term memory, while still allowing synaptic rewiring in order to adapt to changes in external stimuli [16]. A realistic network model of neural activity and plasticity should therefore allow for a broad distribution of firing rates to cope with these functional aspects.

In this paper we examine *diffusive homeostasis* as a possible candidate to replace a previously used model of single-cell intrinsic plasticity. The idea and modeling of diffusive homeostasis was adopted from a paper by Sweeney et al. [18], which models neural tissue as a two-dimensional surface and a set of points representing the neurons' positions. The group of excitatory neurons acted as a point-source of nitric oxide (NO) as well as as a sensor for the NO-concentration at each individual position. The production and sensing of NO forms the basis of a feedback loop: The individual NO-readout is fed into a comparator which causes an appropriate change within the internal firing threshold of the neuron, in turn altering the neuron's firing rate. The control system is then closed by linking the rate of NO-production to the neuron's firing rate. The results by Sweeney et al. suggest that diffusive signaling could resolve the dichotomy between overall stability of firing activity and the need to allow flexibility among individual neurons' activities. Through the diffusive signal, each neurons receives - intuitively speaking - a mixture of its own activity and its neighboring neurons. Individual tuning of firing rates is thereby suppressed while the overall population activity is kept at a constant level.

Key aspects of this paper include an analysis of the stability of the homeostatic control, followed by a comparison of features of the original LIF-SORN and the diffusive variant. We expected to observe a preservation of non-random features that have been found in the original LIF-SORN while incorporating a stronger variance within neural activity which has previously been suppressed by single-cell homeostasis. Furthermore, we predicted excitatory activity on the level of individual cells by an analytic approach, thereby gaining an understanding of the relation between spatial structure and firing rates. In the face of possible new features within the network's structure, we clarify the causal relation between diffusive spatial interaction and synaptic topology.

Materials and methods

0.1 Network Simulation

The Neural Network was simulated with the code used in [11], which makes use of the BRIAN spiking neural network simulator [19]. All following explanations regarding the simulation of neurons and mechanisms of synaptic plasticity are thus based on the methods described in the aforementioned paper.

400 excitatory LIF neurons and 80 inhibitory LIF neurons were assigned random positions across a square area of $1000 \times 1000 \mu m$. All but recurrent excitatory synapses were randomly generated before the start of the simulation until a desired connection fraction was reached. The connection probability between two neurons was calculated from a distant dependent Gaussian function with a standard deviation of $200 \mu m$. For excitatory to inhibitory (EI) and inhibitory to excitatory (IE) synapses, the connection fraction was set to 0.1, and 0.5 for recurrent inhibitory synapses (II). These connections were kept at a fixed connection strength throughout the simulation. Furthermore, all synapses were simulated with a fixed (distance independent) conduction delay. See table 1 for a summary of parameters.

Recurrent excitatory synapses were subject to a number of plastic mechanisms to be described in the following.

parameter	EE	EI	IE	II
connection fraction	→ 0.1	0.1	0.1	0.5
initial connection strength	0.0001mV	1.5mV	−1.5mV	−1.5mV
conduction delay	1.5ms	0.5ms	1.0ms	1.0ms

Table 1. Parameters of synaptic connections.

0.1.1 Synaptic Plasticity

Synaptic Growth: The random, distance dependent generation of new EE synapses was carried out n times once per second, where n is taken from a normal distribution with mean 920 and standard deviation $\sqrt{920}$. This constant growth rate was tuned to achieve the desired target concentration of 0.1 (see 1).

Synaptic Pruning: At the same rate of 1/sec, EE synapses below a threshold of 0.000001 mV were removed, thus being added again to the set of "potential" connections from which the growth process draws new connections.

Spike Timing Dependent Plasticity: An additive STDP rule was used as described e.g. in [5]. The change of weight between two neurons due to a pre- and postsynaptic spike ($i \rightarrow j$) is defined as:

$$\Delta w_{ji} = \sum_k \sum_l W(t_j^l - t_i^k) \quad (1)$$

$$W(\Delta t) = A_+ \exp(-\Delta t / \tau_+), \quad \Delta t > 0 \quad (2)$$

$$W(\Delta t) = A_- \exp(\Delta t / \tau_-), \quad \Delta t < 0 \quad (3)$$

Indexes k and l refer to the k-th and l-th pre- and postsynaptic spike respectively. Parameters were chosen to approximate data from [20] and [21], namely $\tau_+ = 15ms$, $A_+ = 15mV$, $\tau_- = 30ms$ and $A_- = -7.5mV$. However, we used the "nearest neighbor" approximation for the sake of reduction of computational effort, only calculating the effect of the most recent pre-post pair of spikes for potentiation and post-pre pair for depression, yielding roughly the same value as the full summation due to the fast decay times τ_+ and τ_- of the STDP-window.

Synaptic Normalization: We implemented synaptic normalization by calling a function once per sec., updating each w_{ji} from neuron i to neuron j as follows:

$$w_{ji} \rightarrow w_{ji} \frac{w_{total}}{\sum_i w_{ji}} \quad (4)$$

w_{total} was set to different values for each of the four types of connections between the excitatory and inhibitory pool of neurons. Except for the dynamically populated EE-synapses these values could be directly set in accordance with the previously given parameters of desired mean individual connection strength, size of the presynaptic population and connection fraction, by calculating $w_{total} = w_{mean} \cdot N_{presyn.pop} \cdot p_{connect}$. This yielded $w_{total,EI} = 60mV$, $w_{total,IE} = -12mV$, $w_{total,II} = -60mV$. $w_{total,EE}$ was set to $40mV$, corresponding to a mean synaptic weight of $1mV$, given a targeted EE-connection fraction of 0.1 and a population of 400 excitatory neurons.

Short Term Plasticity: A short term plasticity (STP) mechanism acting on recurrent excitatory connections was implemented as presented in [22] as an additional stabilization of network activity. It modulates the effective synaptic weights by multiplying the value stored in the weight matrix w_{ji} by two dynamic variables x and u , $w_{ji}^{effective} = w_{ji} \cdot x \cdot u$, each synapse owning a pair (x, u) . The dynamics of these variables are given by:

$$\dot{x} = \frac{1-x}{\tau_d}, \quad \dot{u} = \frac{U-u}{\tau_f} \quad (5)$$

Each presynaptic spike furthermore causes a change of x and u by

$$x \rightarrow x - x \cdot u, u \rightarrow u + U(1 - u) \quad (6)$$

If no spikes arrive the system rests at $x \cdot u = U$. Otherwise, depending on the choice of τ_d and τ_f , one can achieve a weight modulation that is dominated by potentiation ($\tau_f \gg \tau_d$) or depression ($\tau_f \ll \tau_d$). We chose $U = 0.04$, $\tau_d = 0.5s$ and $\tau_f = 2s$ as a rough approximation of the values that were experimentally observed [22], giving it a tendency towards potentiation. However, one should keep in mind that for $U \in [0, 1]$, $x \cdot u \in [0, 1]$ always holds, thus the factor $x \cdot u$ has a generally diminishing effect. For our choice of variables for example, a Poisson input with a constant rate achieves the best synaptic transmission at a rate of $\sim 4.5Hz$, corresponding to $x \cdot u \approx 0.2$. *Potentiation* in this context refers to the fact that stronger input strengthens synaptic transmission *compared* to close to zero incoming spikes.

0.1.2 Neuron Model

We used a leaky integrate-and-fire-model for all neurons in the network, whose dynamics are described by a stochastic differential equation:

$$\tau_m dV = -(V - E_l)dt + \sqrt{\tau_m} \sigma dW \quad (7)$$

where V is the membrane potential, E_l is the equilibrium membrane potential, τ_m is the time constant of the membrane, σ is the standard deviation of the noise term and dW is the standard Wiener process. A neuron is said to spike when its membrane potential reaches the threshold voltage V_t . The voltage is then reset to V_r . A refractory period was not implemented. A presynaptic spike causes a simple (delayed, see Table 1) increment of the membrane potential of the postsynaptic neuron by $w_{ji}^{effective}$. Table 2 summarizes the aforementioned set of parameters.

0.1.3 Intrinsic Plasticity (IP)

Apart from dynamic processes within synapses which contribute to a stabilization of the network's activity, neurons possess internal mechanisms capable of maintaining a desired regime of activity. Regular-spiking cells are known to down-(up-)regulate their firing rate upon increased (decreased) input on a timescale of tens of milliseconds [23,24]. The network itself was not expected to exhibit fast changes of synaptic input since our simulation did not incorporate any rapidly changing external drive, which allowed us to neglect this feature. On the other hand, a similar form of adaption as a reaction on deprived or enhanced input can be observed on a timescale of hours to days [25]. In the latter case, a long-term change in excitability can be attributed to an altered resistance of ionic channels. This contrasts the former short-term adaption, which can be explained by a separation of timescales among different ionic currents in the cell. A simple form of low intrinsic homeostasis was implemented in the original LIF-SORN by altering the neurons' firing threshold based on the deviation from a target firing rate. During the research reported by this paper we implemented a new model of slow intrinsic homeostasis, based on the work in [18]. The following section describes both models in further detail.

0.1.4 Modeling of Homeostatic Intrinsic Plasticity

Our original model of homeostatic control was described as an operation over discrete time steps $\Delta t = 0.1ms$, carried out for each excitatory neuron:

$$V_t \rightarrow V_t + \eta_{IP}(N_{spikes} - h_{IP}) \quad (8)$$

$$N_{spikes} \rightarrow 0 \quad (9)$$

where V_t is the firing threshold, η_{IP} an adaption rate and h_{IP} the desired number of spikes per time step. N_{spikes} is a variable, counting the number of spikes of the neuron within each interval. In a continuous, rate-based form, this update rule can as well be written as:

$$\dot{V}_t = \eta_{IP}(r - r_{IP}) \quad (10)$$

with r as the neuron's firing rate and $r_{IP} = h_{IP}/\Delta t$ the target firing rate. This feedback control indirectly drives the firing rate of each neuron towards r_{IP} : If $r > (<)r_{IP}$, V_t increases (decreases), reducing (increasing) the probability of a spike to occur.

The new diffusive homeostatic model by Sweeney et al. consists of a set of differential equations:

$$Ca^{2+}_i(t) = -\frac{Ca^{2+}_i}{\tau_{Ca^{2+}}} + Ca^{2+}_{spike} \sum_j \delta(t - t_{spike,i,j}) \quad (11)$$

$$nNOS_i(t) = \frac{1}{\tau_{nNOS}} \left(\frac{Ca^{2+}_i{}^3}{Ca^{2+}_i{}^3 + 1} - nNOS_i \right) \quad (12)$$

$$\dot{NO}(\mathbf{r}, t) = -\lambda NO + D \nabla^2 NO + \sum_i \delta^2(\mathbf{r} - \mathbf{r}_{neur,i}) \cdot nNOS_i \quad (13)$$

$$\dot{V}_{t,i}(t) = \frac{NO(\mathbf{r}_{neur,i}, t) - NO_0}{NO_0 \cdot \tau_{V_t}} \quad (14)$$

A depolarization within a nerve cell upon a spike-event t_{spike} causes a fixed inflow of ionic current Ca^{2+}_{spike} , which is modeled as an instantaneous increase of the Ca^{2+} concentration. The concentration decays exponentially by a time constant $\tau_{Ca^{2+}}$. Though Ca^{2+} currents can be described in a much more detailed fashion, it can be considered as a reasonable approximation [26, p. 198-203]. The influence of Ca^{2+} onto nNOS was modeled by Sweeney et al. through (12) using the Hill equation [27] to model a cooperative binding mechanism. The $nNOS$ production is then fed into the "pool" of nitric oxide via point sources located at the neurons' positions. An additional decay term was added apart from the inflow and the diffusive term to provide a stable finite NO concentration under constant neuronal activity.

Finally, the dynamics of firing thresholds $V_{t,i}$ were modeled such that the rate of change is proportional to the relative deviation of NO concentration at the neurons' locations from a global target concentration NO_0 .

To acquire a target concentration NO_0 corresponding to the desired mean firing rate, we let the system run with the previous homeostatic mechanism, still solving equation (11)-(13) until a steady mean over the concentrations at the neurons' positions was reached. This mean was then set to be the target concentration and we switched to diffusive homeostasis. Table 3 summarizes the choice of parameters that were introduced in this section. Diffusion parameters roughly match those measured in experiments [28].

0.2 Simulation of Diffusion

We solved (13) with the finite difference method on a grid $\mathbf{r}_{i,j}$ with a resolution of 100×100 points. Integration over time was carried out by a 4th-order Runge-Kutta method with a time step of $1ms$. $\nabla^2 NO(\mathbf{r}_{i,j}) = \nabla^2 NO_{i,j}$ was approximated by

$$\nabla^2 NO_{i,j} \approx \frac{NO_{i+1,j} + NO_{i-1,j} + NO_{i,j+1} + NO_{i,j-1} - 4NO_{i,j}}{h^2} \quad (15)$$

on each time step, where $h = L/100$ is the distance between neighbored grid points, determined by the length L of the square sheet and the resolution of the numeric grid. We implemented three possible boundary conditions into the simulation:

1.) Periodic boundary conditions:

$$NO_{i,N+1} = NO_{i,0} \quad (16)$$

$$NO_{N+1,i} = NO_{0,i} \quad (17)$$

$$NO_{i,-1} = NO_{i,N} \quad (18)$$

$$NO_{-1,i} = NO_{N,i} \quad (19)$$

with N being the grid resolution.

2.) Neumann boundary conditions with $\nabla NO = (0, 0)$ at the boundaries:

$$NO_{i,N+1} = NO_{i,N-1} \quad (20)$$

$$NO_{N+1,i} = NO_{N-1,i} \quad (21)$$

$$NO_{i,-1} = NO_{i,1} \quad (22)$$

$$NO_{-1,i} = NO_{1,i} \quad (23)$$

3.) Dirichlet boundary conditions with $NO = NO_{bound}$ at the boundaries.

Neumann boundary conditions were used for most of the simulations if not explicitly marked differently. This decision relates to the previously described mechanism of synaptic growth: Neurons placed close to the edge of the sheet have a lower connection probability due to the absence of neighboring neurons in the direction perpendicular to the close-by border. It therefore models the synaptic growth within a square "cutout" of neural tissue. The Neumann boundary condition fits into this picture since it allows a zero-flux condition at the borders. This is a reasonable assumption, because NO molecules cannot diffuse out of the tissue (unless they were placed in a fluid surrounding).

Equation (13) describes the influx of NO as a sum of scaled and spatially shifted Dirac functions. Apart from the question whether this source term results in a well defined, finite solution at the neurons' positions (see section ??), it can only be modeled to a certain degree of accuracy depending on the resolution of the numeric grid. In practice, we approximated the point sources of NO as an insertions at individual grid cells at a rate of $nNOS_i(t)/h^2$, where the normalizing divisor h^2 ensured the desired total influx per neuron. This numeric implementation required two additional constraints: First, all random neuron positions were confined to integer multiples of h in x- and y-direction. Second, to avoid redundancy and for physiological reasons, each grid cell could only hold one neuron at maximum.

Results

0.2.1 Distribution of Firing Rates

Achieving a broad distribution of firing rates among excitatory neurons was the core motivation for the implementation of diffusive homeostasis. Figure 1 shows a first result, comparing both homeostatic mechanisms. As expected, non-diffusive homeostasis leads to a sharp distribution of firing rates at 3 Hz. Diffusive homeostasis indeed results in a much broader distribution of mean firing rates. As mentioned in the introduction, a large number of experimental studies have found that distributions of firing rates are not only broadly distributed but well described by a log-normal distribution, which has a non-zero third moment or skewness. By definition, the logarithm of the random variable in question is thus again normally distributed. We plotted the the distribution of decadic logarithms of firing rates in Figure 1 (B) to check for this property. In (A), we found a skewness of $v_{Diff} = 0.765$, in (B) $v_{Diff,log} = -0.488$. Though this told us

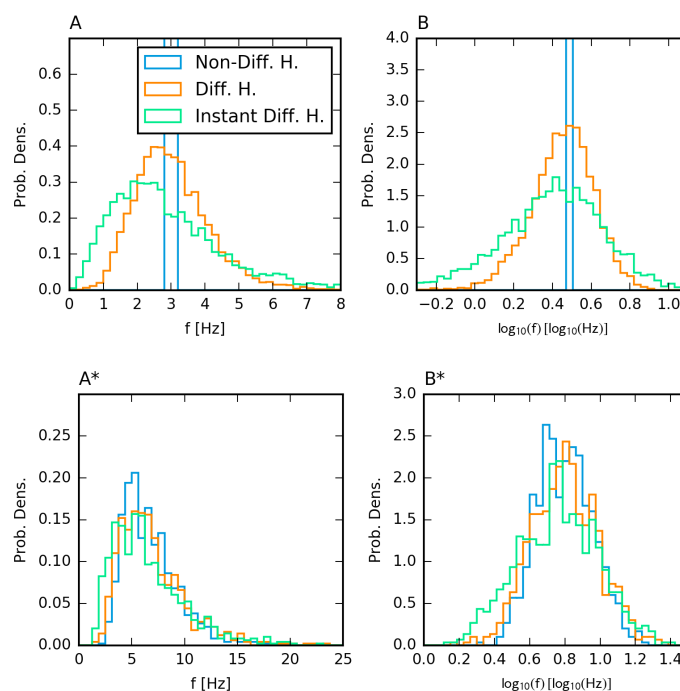


Fig 1. Histograms of mean firing rates over the excitatory/inhibitory population in regular (A/A*) and logarithmic space (B/B*). For diffusive homeostasis ($D = 10 \mu\text{m}^2\text{ms}^{-1}$ and instant), the distribution was generated from 10 simulation runs, 1 simulation was used for non-diffusive homeostasis. Mean firing rates were calculated from spikes within $t = 1000 - 1500$ s.

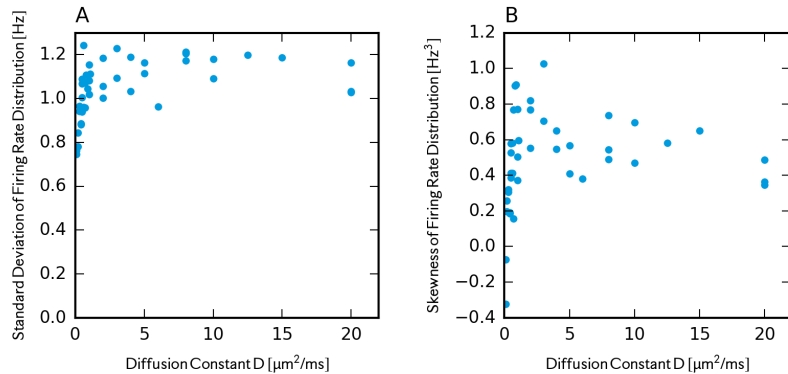


Fig 2. Standard deviation (A) and skewness (B) of firing rate distribution of excitatory neurons (Neumann boundary conditions).

that the distribution is "more symmetric" on a logarithmic scale, it should rather be seen as being neither strictly normally or log-normally distributed.

Sweeney et al. found that diffusive homeostasis maintains broadness of firing rates across a wide range of diffusion constants but rapidly approaching zero for small values [18, p. 6]. We were able to reproduce this result, see Figure 2 (A). Homeostasis reaches a point of saturation, where faster diffusion has no effect on the heterogeneity of firing rates. We also investigated the influence of the diffusion constant onto the distribution's skewness, shown in Figure 2 (B), to further quantify this dependence. Compared to the standard deviation, we saw a similar but not as clear trend with a drop for very small diffusion constants, even occasionally resulting in a left-skewed distribution (negative D-values).

A naturally emerging question when altering the diffusion constant is how the firing rate behaves in the absolute limit of infinitely fast diffusion. In fact, this case is quite easy to implement simulation-wise: One simply has to feed all NO-sources into a single scalar variable of NO concentration. This will provide the same NO readout for all excitatory neurons, which means that all excitatory thresholds change at the same rate all the time, only shifting their initial random distribution. Figure 1 also shows the distribution for this special limiting case. The standard deviation for the excitatory population was $\sigma_{\text{inst}} = 1.79$ Hz and the skewness $v_{\text{inst}} = 1.51$ ($v_{\text{inst},\log} = -0.52$), which makes the asymmetry slightly more pronounced.

0.3 Previously reported features of network topology and dynamics are preserved

While we explicitly intended altering the statistics of excitatory firing rates by implementing diffusive homeostasis, we hoped to preserve what has previously been reported by Miner and Triesch regarding the evolution and structure of recurrent excitatory weights [11]. Figure 3 summarizes features that we found to be preserved for diffusive homeostasis. Diffusive homeostasis leads to the same stable level of recurrent excitatory connection fraction, as well as the observation that a non-uniform connection profile is required to allow for an over-representation of bidirectional connections, as reported previously [11]. A more general discussion on this issue was given by Hoffmann and Triesch [29]. Figure 3,C shows that a log-normal like distribution of excitatory weights is preserved under diffusive homeostasis, though a broader shape could be observed. Figure 3,D illustrates the preservation of a distribution of recurrent excitatory

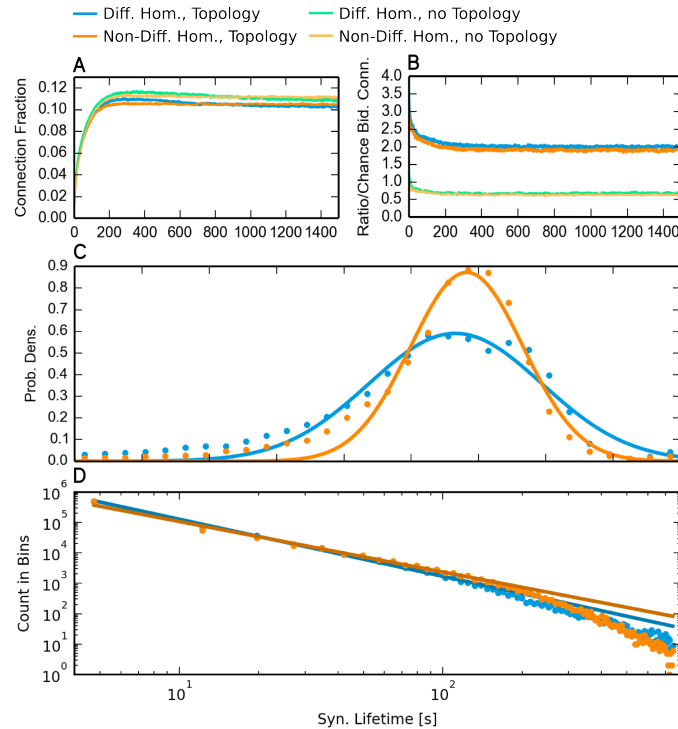


Fig 3. A: Evolution of recurrent excitatory connection fraction. *Topology* refers to the presence or absence of a gaussian connection profile (see Section 0.1.1). B: Ratio of bidirectional connections relative to a random Erdős-Rényi graph. C: Distribution of excitatory recurrent weights after 1500 s. Solid curves are gaussian fits. D: Distribution of recurrent excitatory synaptic lifetimes. Solid lines are linear fits, giving a slope of -1.871 for diffusive homeostasis and -1.676 for non-diffusive homeostasis.

synaptic lifetimes during the steady phase of connectivity, resembling a power-law. Given the assertion that the slope of this distribution is linked to the overall balance of synaptic potentiation and depression [11], we can assume that both types of homeostasis result in a similar net difference between potentiation and depression.

0.4 Broadness of Firing Rate leads to the Emergence of Highly Influential Excitatory Neurons

Having reproduced these results of the previous model, we further sought for possible differences within our network topology as a result of diffusive homeostasis. Since we only implemented synaptic normalization for the sum of ingoing weights, the total or average strength of *outgoing* connections may vary from cell to cell. In a sense, the strength of outgoing connections per neuron can be regarded as a measure of how influential a neuron's activity is with respect to other neurons in the network. Effenberger et al. have shown in computational studies that these "driver neurons" form highly active and interconnected subnetworks [4], an observation that is backed up by experimental studies [30,31]. Figure 4 shows that diffusive homeostasis allows for the emergence of a small group of highly influential neurons, which reproduces the findings in [4]. A comparison of statistics generated with shuffled versions of the weight matrices illustrates that above-chance exceptionally strong outgoing weights were indeed present.

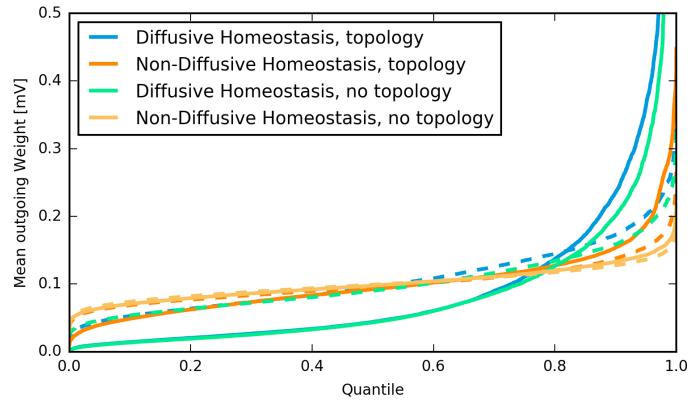


Fig 4. Mean of outgoing weights of excitatory neurons in order sorted by magnitude. Dashed lines are means obtained by randomly shuffling synaptic weights. Data was taken from 25 weight matrices per line, representing weights within $t = 1000 - 1500$ s.

0.5 Spatial Configuration of Neurons allows for the precise Prediction of Firing Rates

After having analyzed the distribution of firing rates resulting from the implementation of diffusive homeostasis, we were interested in how strongly the actual positioning of excitatory neurons influences the resulting statistics of firing activity. To do so, we assumed that the spontaneous firing measured during the "stable phase" of the network, characterized by a constant excitatory connectivity, can be regarded as a homeostatic steady state. Given no sudden strong changes of neural input, the homeostatic feedback levels out the error to approximately zero, since Equation 14 is a realization of an integral control. Our search for the steady-state configuration of firing rates thus reduced to finding a set of firing rates that led to a concentration level of NO_0 at every excitatory neuron's position:

$$NO(\mathbf{x}_{neur,i}) = NO_0, \forall i. \quad (24)$$

Furthermore, we found that the nonlinearity between spiking activity and NO synthesis could be well approximated by a linear relation between average firing rate r_i and rate of NO-synthesis $nNOS_i$ by

$$nNOS_i = \frac{Ca_{spike}^{2+} \tau_{Ca^{2+}} \ln(2)}{3} \cdot r_i \equiv \gamma r_i. \quad (25)$$

See Appendix ??? for a derivation of the proportionality factor. Given this simplification, the steady state of NO concentration is thus defined by the solution of

$$0 = -\lambda NO + D \nabla^2 NO + \sum_i \delta^2(\mathbf{x} - \mathbf{x}_{neur,i}) \cdot \gamma \cdot r_i \quad (26)$$

$$\left(\nabla^2 + \left(i \sqrt{\frac{\lambda}{D}} \right)^2 \right) NO = \sum_i \delta^2(\mathbf{x} - \mathbf{x}_{neur,i}) \cdot \frac{-\gamma \cdot r_i}{D} \quad (27)$$

which is a two-dimensional Helmholtz equation. Its Green's function is

$$NO_i(\mathbf{x}) = \frac{r_i \gamma}{2\pi D} K_0 \left(|\mathbf{x}| \sqrt{\frac{\lambda}{D}} \right) \equiv r_i \cdot \psi_{point}(|\mathbf{x}|) \quad (28)$$

where K_0 is the zeroth modified Bessel function of the second kind [32]. This solution reveals a fundamental problem of modeling the sources of NO-production as point sources: the fact that $K_0(x)$ diverges to infinity for $x \rightarrow 0$. It is merely due to the finite density of the numeric grid used for the simulation of diffusion that allows for a finite target value of concentration.

Generally speaking, no matter how the actual shape of the numeric solution in the equilibrium at a constant production rate looks like, it must be of the form

$$NO_i(\mathbf{x}) = r_i \cdot \psi(d(\mathbf{x}_{neur,i}, \mathbf{x})) \quad (29)$$

$$d(\mathbf{x}, \mathbf{y}) \equiv |\mathbf{x} - \mathbf{y}|. \quad (30)$$

The full solution is then

$$NO(\mathbf{x}) = \sum_i NO_i(\mathbf{x}). \quad (31)$$

By defining

$$\psi_{ij} \equiv \psi_{ij} \equiv \psi(d(\mathbf{x}_{neur,i}, \mathbf{x}_{neur,i})) \quad (32)$$

we could express the condition (24) as

$$\sum_j \psi_{ij} \cdot r_j = NO_0 \quad (33)$$

or, as an operator

$$\hat{\psi} \mathbf{r} = NO_0 \mathbf{n} \quad (34)$$

$$\mathbf{n} \equiv (1, 1, \dots, 1). \quad (35)$$

The problem of finding the steady-state solution of the homeostatic constraint thus reduced to inverting $\hat{\psi}$:

$$\mathbf{r} = NO_0 \hat{\psi}^{-1} \mathbf{n} \quad (36)$$

Still, we had to find a modified, non-diverging version of $\psi(d(\mathbf{x}_{neur,i}, \mathbf{x}))$ to acquire any prediction from this model. It had to retain the shape given by (28) for larger distances but approach the correct numeric error value at the origin, determined by the spacing of the numeric grid. We solved this problem by the following expression:

$$\psi_{approx.} \equiv \frac{1}{\left(\frac{1}{\psi_0^\varepsilon} + \frac{1}{\psi_{point}^\varepsilon} \right)^{\frac{1}{\varepsilon}}} \quad (37)$$

where ε determines the "smoothness" of transition between ψ and the cutoff value ψ_0 . We chose $\varepsilon = 10$ for all further calculations. We took the simple approach of interpreting this value as a mean of the analytic solution across the area covered by the corresponding grid cell to find an expression for ψ_0 . As an additional simplification, we substituted the necessary integration over the square grid cell by a circular area of equal size around the source. This calculation yielded

$$\psi_0 = \gamma \frac{1 - h \sqrt{\frac{\lambda}{\pi D}} K_1 \left(h \sqrt{\frac{\lambda}{\pi D}} \right)}{h^2 \lambda} \quad (38)$$

where h is the spatial resolution of the grid cells.

By simply calculating all matrix elements of $\hat{\psi}$ by means of Equation (32), one would neglect the finite boundaries of the system, which would cause neurons close to the edge to "bleed" into empty space.

Discussion

Nulla mi mi, venenatis sed ipsum varius, Table ?? volutpat euismod diam. Proin rutrum vel massa non gravida. Quisque tempor sem et dignissim rutrum. Lorem ipsum dolor sit amet, consectetur adipiscing elit. Morbi at justo vitae nulla elementum commodo eu id massa. In vitae diam ac augue semper tincidunt eu ut eros. Fusce fringilla erat porttitor lectus cursus, vel sagittis arcu lobortis. Aliquam in enim semper, aliquam massa id, cursus neque. Praesent faucibus semper libero [?].

Conclusion

Maecenas convallis mauris sit amet sem ultrices gravida. Etiam eget sapien nibh. Sed ac ipsum eget enim egestas ullamcorper nec euismod ligula. Curabitur fringilla pulvinar lectus consectetur pellentesque. Quisque augue sem, tincidunt sit amet feugiat eget, ullamcorper sed velit.

Sed non aliquet felis. Lorem ipsum dolor sit amet, consectetur adipiscing elit. Mauris commodo justo ac dui pretium imperdiet. Sed suscipit iaculis mi at feugiat. Ut neque ipsum, luctus id lacus ut, laoreet scelerisque urna. Phasellus venenatis, tortor nec vestibulum mattis, massa tortor interdum felis, nec pellentesque metus tortor nec nisl. Ut ornare mauris tellus, vel dapibus arcu suscipit sed. Nam condimentum sem eget mollis euismod. Nullam dui urna, gravida venenatis dui et, tincidunt sodales ex. Nunc est dui, sodales sed mauris nec, auctor sagittis leo. Aliquam tincidunt, ex in facilisis elementum, libero lectus luctus est, non vulputate nisl augue at dolor. For more information, see S1 Appendix.

Supporting information

S1 Fig. Bold the title sentence. Add descriptive text after the title of the item (optional).

S2 Fig. Lorem ipsum. Maecenas convallis mauris sit amet sem ultrices gravida. Etiam eget sapien nibh. Sed ac ipsum eget enim egestas ullamcorper nec euismod ligula. Curabitur fringilla pulvinar lectus consectetur pellentesque.

S1 File. Lorem ipsum. Maecenas convallis mauris sit amet sem ultrices gravida. Etiam eget sapien nibh. Sed ac ipsum eget enim egestas ullamcorper nec euismod ligula. Curabitur fringilla pulvinar lectus consectetur pellentesque.

S1 Video. Lorem ipsum. Maecenas convallis mauris sit amet sem ultrices gravida. Etiam eget sapien nibh. Sed ac ipsum eget enim egestas ullamcorper nec euismod ligula. Curabitur fringilla pulvinar lectus consectetur pellentesque.

S1 Appendix. Lorem ipsum. Maecenas convallis mauris sit amet sem ultrices gravida. Etiam eget sapien nibh. Sed ac ipsum eget enim egestas ullamcorper nec euismod ligula. Curabitur fringilla pulvinar lectus consectetur pellentesque.

S1 Table. Lorem ipsum. Maecenas convallis mauris sit amet sem ultrices gravida. Etiam eget sapien nibh. Sed ac ipsum eget enim egestas ullamcorper nec euismod ligula. Curabitur fringilla pulvinar lectus consectetur pellentesque.

Acknowledgments

Cras egestas velit mauris, eu mollis turpis pellentesque sit amet. Interdum et malesuada fames ac ante ipsum primis in faucibus. Nam id pretium nisi. Sed ac quam id nisi malesuada congue. Sed interdum aliquet augue, at pellentesque quam rhoncus vitae.

References

1. Lazar A, Pipa G, Triesch J. SORN: a self-organizing recurrent neural network. *Frontiers in Computational Neuroscience*. 2009;3.
2. Savin C, Joshi P, Triesch J. Independent Component Analysis in Spiking Neurons. *PLOS Computational Biology*. 2010;6(4):1–10. doi:10.1371/journal.pcbi.1000757.
3. Tetzlaff C, Kolodziejcki C, Timme M, Wörgötter F. Analysis of Synaptic Scaling in Combination with Hebbian Plasticity in Several Simple Networks. *Frontiers in Computational Neuroscience*. 2012;.
4. Effenberger F, Jost J. Self-Organization in Balanced State Networks by STDP and Homeostatic Plasticity. *PLOS Computational Biology*. 2015;.
5. Zhang LI, Tao HW, Holt CE, Harris WA, Poo M. A critical window for cooperation and competition among developing retinotectal synapses. *Nature*. 1998;395:37–44.
6. Turrigiano GG. The Self-Tuning Neuron: Synaptic Scaling of Excitatory Synapses. *Cell*. 2008;135.
7. Haider B, Duque A, Hasenstaub AR, McCormick DA. Neocortical Network Activity In Vivo Is Generated through a Dynamic Balance of Excitation and Inhibition. *Journal of Neuroscience*. 2006;26(17):4535–4545. doi:10.1523/JNEUROSCI.5297-05.2006.
8. Vogels TP, Sprekeler H, Zenke F, Clopath C, Gerstner W. Inhibitory Plasticity Balances Excitation and Inhibition in Sensory Pathways and Memory Networks. *Science*. 2011;334(6062):1569–1573. doi:10.1126/science.1211095.
9. Abbott L, Nelson SB. Synaptic Plasticity: taming the beast. *Nature Neuroscience*. 2000;.
10. LeMasson G, Marder E, Abbott LF. Activity-dependent regulation of conductances in model neurons. *Science*. 1993;259(5103):1915–1917. doi:10.1126/science.8456317.
11. Miner D, Triesch J. Plasticity-Driven Self-Organization under Topological Constraints Accounts for Non-Random Features of Cortical Synaptic Wiring. *PLoS Computational Biology*. 2016;.
12. Zheng P, Dimitrakakis C, Triesch J. Network Self-Organization Explains the Statistics and Dynamics of Synaptic Connection Strength in Cortex. *PLOS Computational Biology*. 2013;.
13. Markram H. A network of tufted layer 5 pyramidal neurons. *Cerebral Cortex*. 1997;7(6):523–533. doi:10.1093/cercor/7.6.523.

14. Song S, Sjöström PJ, Reigl M, Nelson S, Chklovskii DB. Highly Nonrandom Features of Synaptic Connectivity in Local Cortical Circuits. *PLOS Biology*. 2005;3(3). doi:10.1371/journal.pbio.0030068.
15. Hartmann C, Lazar A, Nessler B, Triesch J. Where's the Noise? Key Features of Spontaneous Activity and Neural Variability Arise through Learning in a Deterministic Network. *PLOS Computational Biology*. 2016;11(12):1–35. doi:10.1371/journal.pcbi.1004640.
16. Buzsáki G, Mizuseki K. The log-dynamic brain: how skewed distributions affect network operations. *Nature Reviews Neuroscience*. 2014;.
17. Wöhrer A, Humphries MD, Machens C. Population-wide distributions of neural activity during perceptual decision-making. *Progress in Neurobiology*. 2012;.
18. Sweeney Y, Kotaleski JH, Hennig MH. A Diffusive Homeostatic Signal Maintains Neural Heterogeneity and Responsiveness in Cortical Networks. *PLoS Computational Biology*. 2015;.
19. Brette R, Goodman D, Stirnberg M. The Brian spiking neural network simulator (Version 1.0) [Computer Software]; 2016. <http://www.briansimulator.org/>. Available from: <http://www.briansimulator.org/>.
20. Bi G, Poo M. Synaptic Modifications in Cultured Hippocampal Neurons: Dependence on Spike Timing, Synaptic Strength, and Postsynaptic Cell Type. *The Journal of Neuroscience*. 1998;18(24):10464–10472.
21. Froemke RC, Poo M, Dan Y. Spike-timing-dependent synaptic plasticity depends on dendritic location. *Nature*. 2005;434(7030):221–225.
22. Markram H, Wang Y, Tsodyks M. Differential signaling via the same axon of neocortical pyramidal neurons. *Proceedings of the National Academy of Sciences*. 1998;95(9):5323–5328.
23. Connors BW, Gutnick MJ. Intrinsic firing patterns of diverse neocortical neurons. *Trends in Neurosciences*. 1990;13(3):99 – 104. doi:[http://dx.doi.org/10.1016/0166-2236\(90\)90185-D](http://dx.doi.org/10.1016/0166-2236(90)90185-D).
24. Benda J, Herz AVM. A Universal Model for Spike-Frequency Adaption. *Neural Computation*. 2003;15(11):2523–2564.
25. Desai NS, Rutherford LC, Turrigiano GG. Plasticity in the intrinsic Excitability of Cortical Pyramidal Neurons. *Nature Neuroscience*. 1999;2:515–520.
26. Dayan P, Abbott LF. *Theoretical Neuroscience*. MIT Press; 2001.
27. Hill A. The possible effects of the aggregation of the molecules of haemoglobin on its dissociation curves. *The Journal of Physiology*. 1910;40:iv—vii. doi:10.1113/jphysiol.1910.sp001389.
28. Philippides A, Husbands P, O'Shea M. Four-Dimensional Neuronal Signaling by Nitric Oxide: A Computational Analysis. *Journal of Neuroscience*. 2000;20(3):1199–1207.
29. Hoffmann FZ, Triesch J. Non-random network connectivity comes in pairs. *Network Neuroscience*. 2017;.

30. Yassin L, Benedetti BL, Jouhanneau JS, Wen JA, Poulet JF, Barth AL. An Embedded Subnetwork of Highly Active Neurons in the Neocortex. *Neuron*. 2010;68(6):1043 – 1050. doi:<http://dx.doi.org/10.1016/j.neuron.2010.11.029>.
31. Eckmann JP, Jacobi S, Marom S, Moses E, Zbinden C. Leader neurons in population bursts of 2D living neural networks. *New Journal of Physics*. 2008;10. doi:10.1088/1367-2630/10/1/015011.
32. Couto RT. Green's functions for the wave, Helmholtz and Poisson equations in a two-dimensional boundless domain. *Revista Brasileira de Ensino Física*. 2013;.

parameter	exc. neur.	inh. neur.
E_l	−60 mV	−60 mV
τ_m	20 ms	20 ms
V_r	−70 mV	−60 mV
σ	$\sqrt{5}$ mV	$\sqrt{5}$ mV
V_t	subject to IP	−58 mV

Table 2. Parameters of LIF neuron

parameter	value
r_{IP}	3 Hz
η_{IP}	0.1 mV
Ca_{spike}^{2+}	1
$\tau_{Ca^{2+}}$	10 ms
τ_{nNOS}	100 ms
D	default: $10 \mu m^2 ms^{-1}$
λ	$0.1 s^{-1}$
τ_{V_t}	see section ??

Table 3. Parameters of homeostatic intrinsic plasticity.